Mw 7.1 Duzce Earthquake: Multiple datasets and implications about rupture kinematics

A. Ozgun Konca[1], Sebastien Leprince[1], Jean-Philippe Avouac[1], Don Helmberger[1]
[1]Tectonic Observatory, California Institute of Technology e-mail: ozgun@gps.caltech.edu

1. Introduction

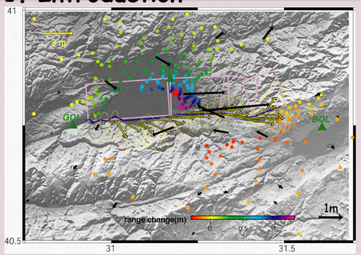

Figure 1a: The Mw7.4 Duzce earthquake data . The black arrows show the GPS offsets, the colored circles show the range change, the green triangles show the strong-motion station locations, the blue curve shows the SPOT obtained fault trace and the yellow vectors show the offset.

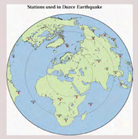

Figure 1b: Location of teleseismic stations for the Duzce earthquake

Datasets used:
1. Campaign GPS data
2. InSAR data
3. SPOT fault map and
4. Surface offset data
5. Strong-motion data
6. Teleseismic data

TARGET

By modeling all available data together, can we learn more about the source of the Duzce event?

Especially, resolve the details about rupture velocity by modeling the near-field seismic data , but also making sure that

1. the fault geometry and surface offsets are consistent with SPOT data
2. slip model fits the geodetic data

2. Background and former studies

2a. NAF and Izmit and Duzce earthquakes

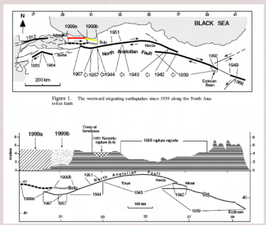

Barka et al., 2002

Figure 2: The North Anatolian fault and the western migration of events in 20th century. The Mw7.4 Izmit earthquake occured on August 17, 1999 (1999a) and Mw7.4 Duzce earthquake occured on Nov 12, 1999 (1999b). Both earhtquakes created significant surface offset and were mapped by field geologists

2b. Supershear rupture Speeds

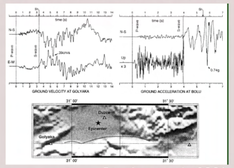

Bouchon et al., 2001

Figure 3: P-S differential timing from strong-motion seismograms of the Duzce earthquake

Supershear rupture velocity was first suggested by Bouchon et al.,2001 for the Duzce Eq. Idea is based on P-S

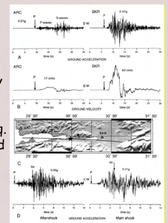

2c.Slip Models from Various Datasets

Figure 4: Various models from various datasets are shown. All the models use a single plane.

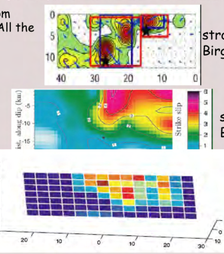

strong-motion Birgoren et al., 2004

strong-motion and GPS Bouin et al., 2004

GPS and InSAR Burgman et

3. Fault map from SPOT subpixel correlation

Figure 5: Cross-correlation of SPOT images from 3 images. (a) June 1999, December 2000 (b) September 1999, December 2000. Insets show the offsets at A-A', B-B' and C-C'.

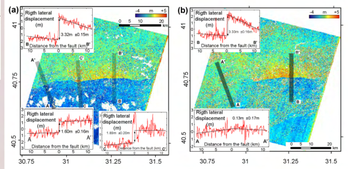

Figure 6. (a) Comparison of surface fault ruptures determined from the sub-pixel correlation of the SPOT images (red lines), observed in the field reported by Pucci et al., 2007 (blue dots). Cumulative distance along the fault is indicated.

(b) Comparison of right lateral fault slip along the main fault trace measured in the field (blue circles with error bars) and from correlating the SPOT images (red, green and black curves) and ignoring the fault strand with apparent left-lateral slip North of Eften lake.

The black curve shows the distribution of fault slip derived from cross-correlating images 1 and 2, and therefore represents the effect of Izmit earthquake only.

The green curve shows the distribution of fault slip due to the Duzce earthquake alone derived from substracting the fault slip due to the Izmit earthquake from the cumulative fault slip.

(c) Comparison of right lateral fault slip along the main fault trace measured in the field (blue circles with error bars) and from correlating the SPOT images (red, green and black curves) and taking into account the fault strand with apparent left-lateral slip North of Eften Lake. The black curve shows the distribution of fault slip derived from cross-correlating images 1 and 2 and therefore represents the effect of Izmit earthquake only. The red curve shows the distribution of fault slip derived from cross-correlating images 2 and 3 representing the effect of Duzce earthquake only. The green curve shows the distribution of fault slip derived from cross-correlating images 1 and 3 and therefore represents the cumulative effect of Izmit and Duzce earthquakes.

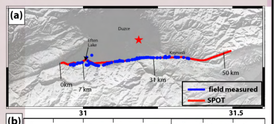

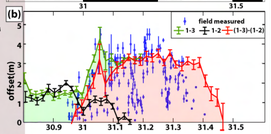

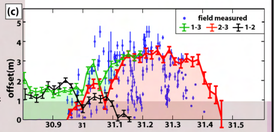

Figure 7: 4 segment fault model based on the SPOT obtained fault map with surface offsets constrained. All models shown later have this fault geometry and dip of 65 degrees.

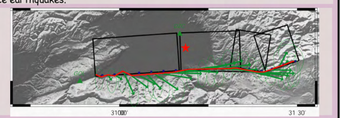

4. Modeling of strong-motion, GPS and InSAR

We have searched for the best fit rupture velocity, to confirm whether supeshear rupture velocities occured to the east. The slip models with different fixed rupture velocities and varying rupture velocities show a very consistent slip pattern due to constraints coming from geodesy.

It is important to note that the rise time is at the limiting value of 6.5 s in significant portion of the fault. Long rise times are also evident from This is also observed in the long duration of slip accumulation at the DZC station. This might imply that the mechanics of Duzce earthquake is more similar to a crack than a slip pulse.

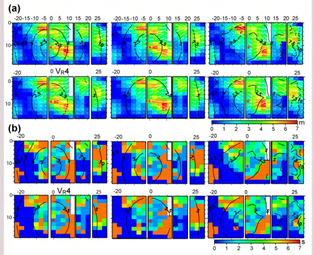

Figure 8: The slip map (top) and rise times (bottome) forjoint models with different rupture velocity constrains.

5. Fits to the strong-motion data

When we look at the fits to the seismograms, it is clear from the station BOL (east of the rupture) that the frequency content of the seismograms can only be obtained by varying rupture velocity runs. None of the constant rupture velocity models fit the BOL data, especially in high frequencies as shown by velocity and accelerations.

Why does BOL have more Sensitivity?

We are pinning down slip very well so it cannot trade off with rupture velocity. However stations very close to the fault record very local time history. There are enough parameters (rise time of each subfault) to account for fitting the data with different rupture velocities. Since BOL is off the fault and it records more global

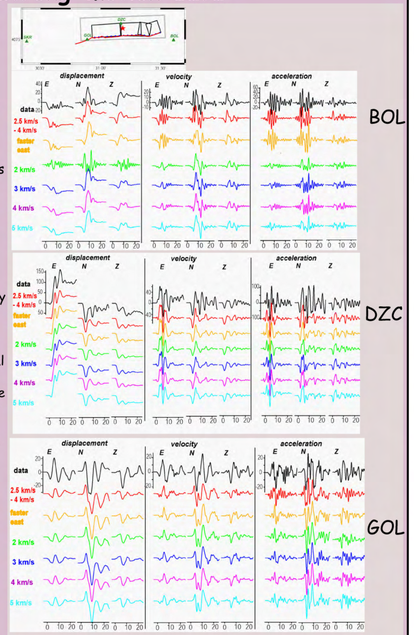

Figure 9:The fits to the strong-motion data, BOL, DZC and GOL from top to bottom. "Faster east" model has 2-3km/s rupture velocity constrain to the west and 2-4.5km/s to the west

6. Snapshots of rupture

Supershear rupture is only significant in east direction.

The rupture toward east starts subshear, accelerates to supershear speeds. Rupture is locally larger than 4 km/s betwen 2 s and 6 s and slows down towards the end. Overall rupture speed toward east is 3.8 km/s, while it is 3 km/s toward west.

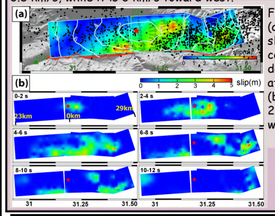

Figure 10:
(a) Map view of total slip with time contours. The black dots represent the aftershock locations.
(b) accumulated slip at 2 second time windows.

7.Fits to the geodetic data

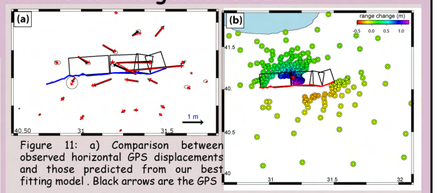

Figure 11: a) Comparison between observed horizontal GPS displacements and those predicted from our best fitting model . Black arrows are the GPS data with their 2-σ uncertainties and red arrows are synthetics.
(b) Comparison between observed LOS displacements and those predicted from our best fitting model (labeled VREf_Ws in Table 4). Each data point is represented by a color coded circle, where the outer larger circle is the observed value and inner circle is the model prediction.

8. Effect of fault geometry on teleseismic models

Now we test the effect of fault geometry on the estimation of near-field ground motion. We test two fault geometries, a single plane based on GCMT strike and dip, and a 4-segment geometry based on our SPOT analysis. Our results show that the teleseismic slip distributions differ significantly when fault geometry is changed (Figure 12). Moreover, the model with 4 segments and surface constraints predicts the near-field seismograms the best (Figure 13). PGV predicted from 4 segment with surface constraints is also most similar to the PGV obtained using all the near field data.

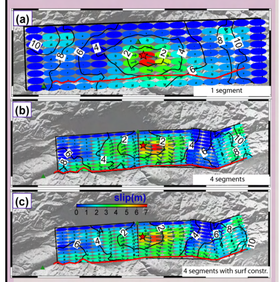

Figure 12: The mapview of models (a) 1-segment teleseismic inversion, (b) 4 segment teleseismic inversion, and (c) 4 segments, teleseismic inversion with constraints on surface slip.

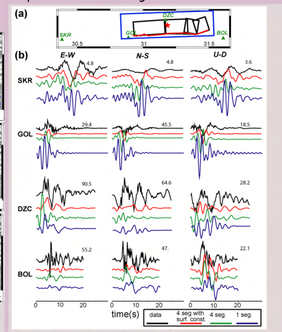

Figure 13. (a) The geometry of the 2 models and the locations of strong-motion stations (b) Predictions of strong motion data from 1-segment and 4-segment models. Unfiltered strong-motion data is shown in black with the peak amplitude shown in cm/s on top of the waveforms.

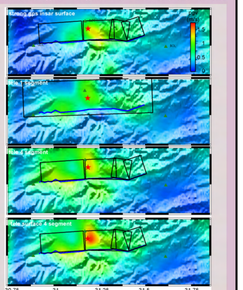

Figure 14. Peak ground velocity (PGV) maps predicted from the best fitting model derived from the inversion of the strong motion and geodetic data (top, model VREf_Ws in Table 4) and from the inversion of the teleseismic data assuming either a single planar fault or a more realistic 4-segment fault geometry and with or without constraints on surface fault slip.

9. Summary and Conclusions

1. We have obtained the detailed surface rupture and offsets of Duzce Earthquake using cross-correlation of SPOT images before and after the earthquake.
2. The Duzce rupture has extended 10 km further east than previously reported field observations.
3. We have modeled the earthquake with all available near-source geodetic and seismic data using an accurate fault geometry based on image cross-correlation.
4. Rapid variations in rupture velocity are required to explain the strong-motion records at BOL station.
5. The long rise time of up to 7 s indicate that Duzce earthquake is more like a crack than a pulse-like rupture.
6. Supershear rupture velocity occurs only toward the east of the hypocenter.
7. Teleseismic models utilizing more accurate fault geometry and surface offsets from satellite imagery predicts the near field data much better and may contribute to the better estimation of rapid